Extending Ground-Based Gravitational-Wave Sensitivity to 5 Hz

Amit Singh Ubhi,[1,*] Lari Koponen,[1] Jiri Smetana,[1] Yulin Xia,[2] Haixing Miao,[2] Emilia Chick,[1] John Bryant,[1] Geraint Pratten,[1] Teng Zhang,[1] Richard Mittleman,[3] Peter Fritschel,[3] Alan V. Cumming,[4] Giles Hammond,[4] and Denis Martynov[1]

[1]*Institute for Gravitational Wave Astronomy, School of Physics and Astronomy, University of Birmingham, Birmingham B15 2TT, United Kingdom*
[2]*Department of Physics, Tsinghua University, Beijing 100084, China*
[3]*LIGO Laboratory, Massachusetts Institute of Technology, Cambridge, Massachusetts 02139, USA*
[4]*Institute for Gravitational Wave Research, School of Physics and Astronomy, University of Glasgow, Glasgow G12 8QQ, United Kingdom*

(Received 2 March 2026; accepted 10 June 2026; published 16 July 2026)

Extending the sensitivity of terrestrial gravitational-wave detectors below 20 Hz is a long-standing challenge, limited by ground motion and inertial sensing noise. In this Letter, we demonstrate ultra-high-vacuum compatible inertial isolation and position sensing technologies that achieve active platform stabilization down to 10 mHz. Our laser position sensors reach a sub-pm/$\sqrt{\text{Hz}}$ sensitivity above 10 mHz, independent of the input light polarization, representing a 100-fold improvement over the current LIGO position sensors. In addition, our inertial sensors provide at least a factor of 5 improvement in low-frequency sensitivity compared to state-of-the-art commercial seismometers. We integrate these technologies into a LIGO-like interferometer model and predict a low-frequency sensitivity improvement of up to an order of magnitude at 10 Hz, with enhanced linearity and calibration stability. This extension increases the detection horizon for intermediate-mass black hole binaries of mass $10^3 M_\odot$ by a factor of 3 and increases the SNR for all lower mass binaries. Our results provide the first experimental demonstration of a practical pathway to sub-10 Hz operation of terrestrial gravitational-wave detectors and establish key technologies for next-generation observatories such as Cosmic Explorer and Einstein Telescope.

DOI: 10.1103/65gz-dcjz

Introduction—Intermediate mass black holes (IMBHs) with masses between $100M_\odot - 10^5 M_\odot$ occupy a critical but largely unexplored gap between stellar mass and supermassive black holes [1]. Only two direct measurements of low-mass IMBHs have been confirmed from gravitational wave (GW) events GW190521 [2] and GW231123 [3], providing compelling evidence for the existence of such objects. Their detections challenge conventional models of stellar evolution and black hole formation [4–6], where the formation pathways bridging stellar mass and supermassive black holes are poorly understood. Detection and characterization of IMBHs are essential for constraining black hole growth channels, testing hierarchical mergers, and probing the evolution of the Universe's most massive compact objects, including the upper mass gap ($50M_\odot - 130M_\odot$) [7–9]. The emission frequency of GWs scales inversely with the total source mass. Therefore, improving low-frequency sensitivity in terrestrial detectors such as LIGO [10–14] is essential to detect IMBHs.

Beyond IMBH detection, improved low-frequency sensitivity also enhances the signal-to-noise ratio (SNR) for lower-mass binaries, extends the premerger observation time, and sharpens sky localization of sources. These gains increase the precision of parameter estimation, enable earlier alerts for multimessenger follow-up [15,16], and reduce degeneracies in inferred source properties, maximizing the scientific return of gravitational-wave observations.

In this Letter, we demonstrate three technologies that together will reduce the residual motion of all suspended optics in the detectors via reduced input motion and sensing noise. These technologies, combined, are critical for future upgrades [17,18] and third-generation detectors [18–22] due to stringent requirements for low-frequency seismic isolation [23–25] and suspension controls [26,27]. We simulate improved strain sensitivity [28–31] from their integration below 30 Hz (Fig. 1), achieving fundamental sensitivity limits in LIGO, and quantify their impact on IMBH detection and parameter estimation (Fig. 5). See Supplemental Material [32] for a breakdown of the noise contributions to the strain sensitivity.

*Contact author: a.s.ubhi@bham.ac.uk

Published by the American Physical Society under the terms of the Creative Commons Attribution 4.0 International license. Further distribution of this work must maintain attribution to the author(s) and the published article's title, journal citation, and DOI.

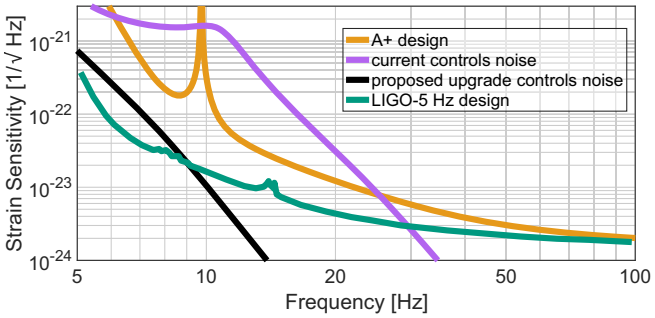


FIG. 1. Detector strain sensitivity comparison for the A+ design (modeled using pyGWINC [33]) and LIGO-5 Hz design [17]. The technical noise with the current inertial isolation schemes is shown in violet. The estimated improvement in the technical noises using our technologies (black) will enable the A+ design sensitivity to be reached, and demonstrates a clear pathway for terrestrial GW detection at 5 Hz.

Technologies—The LIGO detectors use a combination of active and passive inertial isolation systems to minimize motion of their suspended optics [23–25,34]. Active stabilization is achieved by controlling in-vacuum platforms that support the test masses and other core optics, including the beam splitter, and power- and signal-recycling cavity mirrors. The sensitivity of the inertial sensors on the platform determines its residual motion. Furthermore, active damping of the suspension resonances [26,27,34] is required to reduce their rms motion. IMBH detection requires a reduction in the sensing noise of both the active platforms and the suspensions [17]. Recent improvements in the 3–30 Hz band have been demonstrated though optimization of control loop shapes using reinforcement learning methods [35]. In contrast, we focus on hardware-based sensing upgrades that reduce the fundamental sensing noise. These upgrades extend low-frequency performance toward the requirements of next-generation detectors.

The first technology is the compact interferometric laser position sensor (LPS) [36,37], designed to replace the optical shadow sensors [26,27] currently used for local damping of the suspension systems.

The LPS employs a standard telecom distributed feedback laser and deep frequency modulation interferometry [38,39] in an unequal-arm Michelson configuration. The interferometric signal is encoded at the modulation frequency and its harmonics, enabling ac readout that shifts the measurement band away from low-frequency technical noises, and requires only one measurement channel for fringe counting. This sensor achieves a broadband sensitivity of 3×10^{-13} m/$\sqrt{\text{Hz}}$ [Fig. 2(a)]—an improvement of ≈100 compared to the optical shadow sensors.

The key novelty of our design is the pentaprism beam splitter, which completely contains the reference arm of the interferometer. The reference and sample beams then interfere with an offset from the input beam. This decouples reflected light from the optical fiber and suppresses nonlinearities and excess noise caused by parasitic interference [37].

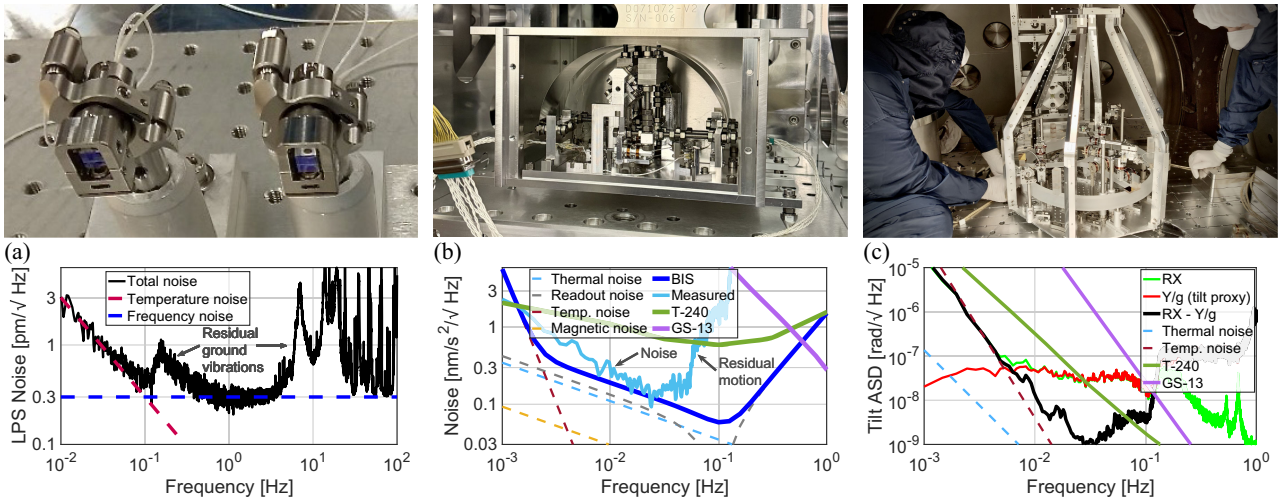


FIG. 2. Photos of the three technologies and their respective noise budgets below. (a) Measured noise for the LPS (black). Subtraction of two sensors enables common-mode rejection of the dc-coupled laser frequency noise in the difference channel. Below 100 mHz the noise is dominated by temperature couplings (dark red), whereas the high-frequency noise floor is dominated by down conversions of laser frequency noise from kHz demodulation (blue). Residual seismic couplings are present at the microseism and above 7 Hz. (b) Noise budget for the BIS. Low frequency sensitivity is limited by direct temperature couplings. In the mid-frequencies, readout and thermal noises limit the device, with readout noise dominating above 0.1 Hz. The total simulated noise is shown in solid blue. The measured noise (solid cyan) is limited by residual motion above and the quality of the subtraction between multiple sensors. The T-240 (dark green) and GS-13 (violet) noises are shown for reference. (c) Noise budget for the tilt degree of freedom for C-6D. Classical temperature noise limits the sensitivity below 10 mHz. Above 30 mHz we sit on the horizontal motion used to subtract the low frequency tilt motion (RX-Y/g) to access the noise floor (black). The T-240 (dark green) and GS-13 (violet) noise are shown for reference.

Furthermore, the LPS is designed to be intrinsically insensitive to input polarization. In fiber-coupled systems, polarization rotation is unavoidable on the timescale of one year due to temperature fluctuations and stress relaxations even with the use of polarization-maintaining fibers. We mitigate the effect of polarization drifts by matching the optical paths of the S- and P-polarization states.

Beyond the intrinsic optical robustness of the LPS design, deployment to measure the six degrees of freedom (d.o.f.) of a suspended mass enables a sensing geometry in which common low-frequency laser frequency noise is subtracted in four of the six d.o.f.s. This removes the need for additional reference sensors and auxiliary control loops, reducing system complexity and easing integration into the detectors.

The next two technologies in our inertial isolation package are advanced inertial sensors that suppress low-frequency motion. Commercial state-of-the-art seismometers do not provide the low-frequency sensitivity at the microseism to enable the platform control sufficient for IMBH astrophysics. We begin with the Birmingham inertial sensor (BIS), which is designed to integrate into the active platforms from which the input, output, power-recycling, and signal-recycling optics are suspended. The BIS is more than an order of magnitude more sensitive below 0.1 Hz than the Geotech Instruments GS-13 sensor currently used on these platforms. In the critical 10–100 mHz frequency band, the BIS sensitivity surpasses the industry-leading Nanometrics Trillium (T-240) seismometer by a factor of 5.

The design is based on the Wielandt-Streckeisen approach [40], employing leaf springs whose shear force provides a tunable antispring. In addition to sensitivity, a key advantage of our sensor is its ultra-high-vacuum compatibility. In-vacuum operation suppresses the limiting thermal noise caused by the readout capacitor plates in state-of-the-art seismometers and simplifies the integration into the LIGO chambers. The BISs are tuned to have a long period of $\approx$15 s, improving the low-frequency readout noise. We position the sensors in pairs inside aluminum and mu-metal shields to suppress temperature fluctuations and reject external magnetic fields. A photo and noise budget for the BIS is shown in Fig. 2(b). Three pairs of BISs enable low-frequency readout and control of six d.o.f.s of the active platforms. See Supplemental Material [32] for a breakdown of the BIS noise measurement.

The final sensor is the fused silica six-degree-of-freedom (six-axis) seismometer (C-6D) [41–45] developed for stabilization of LIGO's test masses and beam splitter. The tilt sensitivity of our sensor is $\leq 10^{-8}$ rad/$\sqrt{\text{Hz}}$ at 10 mHz, a factor of 30 better than the state-of-the-art T-240 seismometer. The tilt noise budget is shown in Fig. 2(c).

The proof mass of C-6D is a fused silica ring with a low index of thermal expansion ($< 5 \times 10^{-7}$/K) suspended by a fused silica fiber with a low mechanical loss angle ($< 10^{-6}$) [46]. This proof mass has eigenfrequencies of 1.5, 9, and 17 mHz for the critical rotational d.o.f.s, which are tuned to minimize the coupling of the sensing noise and simplify the platform control. The proof mass is sensed by six LPSs and its low-frequency drifts (< 1 mHz) are stabilized using coil-magnet actuators.

Platform stabilization—Most active platforms suppress external vibrations from 0.1–1 Hz and inject the sensor noise at lower frequencies [47–51]. We demonstrated the performance of our sensors at LIGO's MIT facility, achieving inertial isolation in all six d.o.f.s. We utilize the same general control strategy as discussed in Ref. [23] with the addition of our sensors. See Supplemental Material [32] for details on the control strategy. The results show that the sensors are not only highly sensitive as discussed above, but can also be robustly diagonalized for platform sensing.

The low-frequency longitudinal control of LIGO's active seismic isolation platforms is limited by tilt-to-horizontal coupling in the platforms' inertial sensors [52–54]. This coupling scales as g/ω^2, degrading the isolation at the microseism and further injecting noise below 0.1 Hz. Both the BIS and C-6D surpass the tilt sensitivities of LIGO's current inertial sensors as we have shown in Figs. 2(b) and 2(c). This improvement directly translates into enhanced low-frequency longitudinal suppression, with the BIS reducing microseismic motion at 0.2 Hz by a factor of 20 in the vertical d.o.f. and a factor of 4 in the horizontal d.o.f.s. In the case of C-6D, we demonstrate the first ever longitudinal platform suppression down to 10 mHz, as shown in Fig. 3(c).

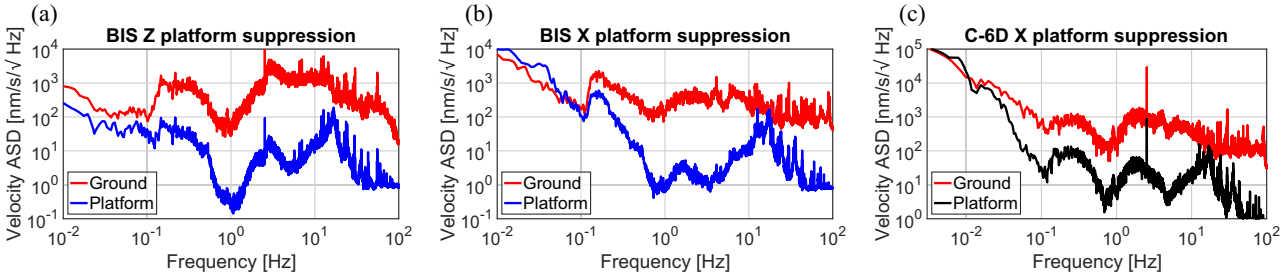


FIG. 3. Active platform stabilization at LIGO's MIT facility. Red traces are the measured ground motion using the out-of-vacuum Streckeisen STS-2 seismometer. The blue (BISs in-loop) and black (C-6D in-loop) traces show the measured platform motion using a T-240 seismometer as a witness sensor. (a) Z degree of freedom. (b) X degree of freedom. (c) X degree of freedom.

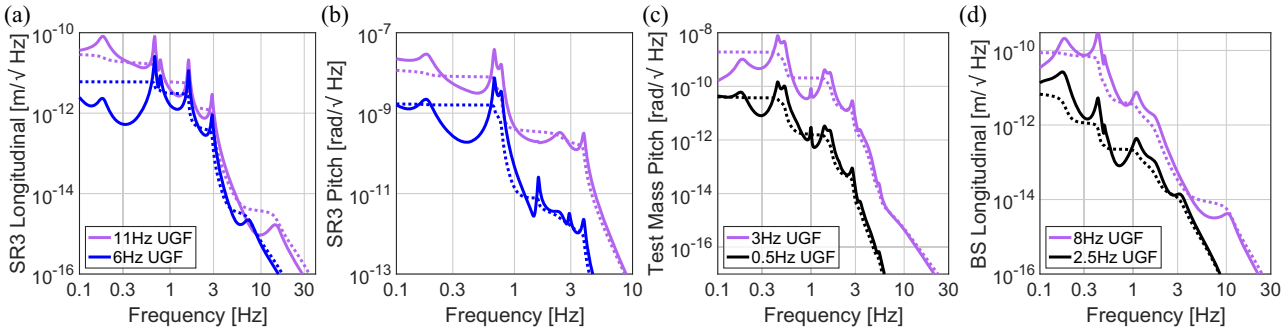


FIG. 4. Comparison of different simulated optic motion when using the BISs (blue) and C-6D (black) in-loop to stabilize the relevant active platforms, and LPSs for suspension damping. The violet traces represent the current motion using the current control scheme with commercial seismometers and optical shadow sensors. The dotted lines represent the rms motion. (a) Signal-recycling cavity telescope optic (SR3) longitudinal motion. (b) SR3 pitch motion. (c) Test mass pitch motion for an individual optic. (d) Beam splitter longitudinal motion.

Detector improvements—The technologies have the potential to improve the sensitivity, linearity, and calibration of LIGO and next-generation GW detectors. We estimate these improvements by simulating the motion of the active platforms when using BIS and C-6D, and propagating the motion through the suspension chains of key optics, which are stabilized using LPSs. The resulting detector sensitivity is shown in Fig. 1, and the astrophysical gains are illustrated via improved detection rate, range, source mass, and IMBH parameter estimation (Fig. 5).

Two key control noises dominate the GW strain sensitivity below 30 Hz [30,55]. First, angular sensing and control must stabilize the motion of the arm cavity mirrors to maintain a stable cavity axis. This is necessary due to the large optical power which can lead to radiation-pressure-induced angular instabilities [56,57]. The second dominant noise arises from length sensing and control, primarily due to longitudinal beam splitter motion. Feedforward to the test masses [58] partially mitigates this, however, the high bandwidth of the control loops [59] leads to noise injection into the GW detection band. Integration of C-6D and LPSs reduces the control bandwidths from 3 to 0.5 Hz for test mass pitch, and 8 to 2.5 Hz for Michelson length control, while simultaneously reducing the rms motion of the optics by a factor of 10 [Figs. 4(c) and 4(d)]. This suppresses control noise injection below the detector's low-frequency noise floor.

Next, we examine the power- and signal-recycling cavities, which directly impacts the power build up in the 4-km long cavities, the optical gain of the GW signal, and the detector linearity [60,61]. Both recycling cavities embed folded telescopes that reduce the beam size from ≈6 cm down to 1 mm. Angular motion of the telescope mirrors changes the position and angle of the optical axes of the recycling cavities. This process couples noise, such as laser frequency and intensity noise, into the GW channel, modulates the antenna response, and compromises detector calibrations. Implementation of BISs and LPSs will reduce the rms longitudinal and pitch motion of the telescope optic by a factor of 5 [Figs. 4(a) and 4(b)] and suppress output pointing fluctuations [28,62] by the same factor. This reduces parasitic coupling of the control sidebands' higher-order modes into the gravitational-wave channel and improves the detector linearity [63]. See Supplemental Material [32] for noise budgets of the optic motion.

With C-6D, BISs, and LPSs deployed on all platforms and suspensions, the residual motion of every suspended optic would be reduced in all d.o.f.s. This would suppress low-frequency technical noises, including auxiliary length and alignment controls, suspension actuation and damping noise [26,27], and scattered light [17,64,65]. Reduced low-frequency platform motion would also minimize fringe wrapping and associated sensing nonlinearities [66], further suppressing control-induced noise and enabling operation at the LIGO design sensitivity (Fig. 1).

Astrophysical gains—The low-frequency sensitivity improvements provide broad astrophysical gains across compact-binary systems. This includes enhanced detection rates, improved parameter estimation, and earlier inspiral access. We highlight the impact on IMBHs, for which the horizon and range increase substantially. See Supplemental Material [32] for the horizon and range comparison, which includes Ref. [67]. We quantify the improvement by using the Fisher information matrix to estimate the statistical uncertainties associated with the binary parameters following the analysis in [18], assuming a two-detector network consisting of LIGO Hanford and LIGO Livingston. The Fisher matrix is calculated using GWFish [68] and the IMRPhenomXHM waveform model [69,70]. With few observational constraints, the functional form of the IMBH population is very poorly constrained and any figure of merit will depend on the assumed population. We generate a mock population assuming 1 yr of observation, with component masses drawn from a power-law distribution as in [18], isotropic spins with uniform magnitudes, and a merger rate following the Madau-Dickinson star formation

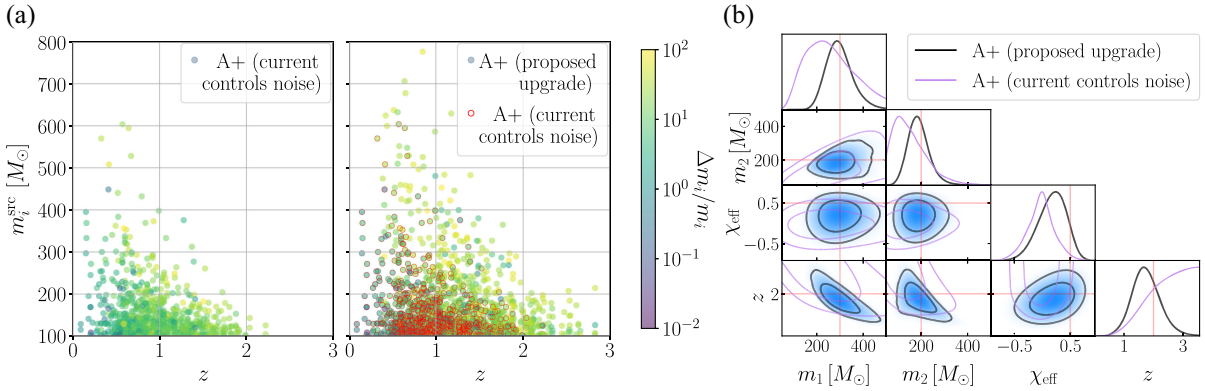


FIG. 5. (a) Left: fractional error on the detector-frame masses as a function of redshift for the A+ configuration with the current controls noise. Right: comparison between the A+ configuration with the current control noise (red circles) and A+ design sensitivity when the proposed upgrade is implemented (colored circles). (b) Parameter estimation comparison for an IMBH merger with source-frame masses of $300M_\odot$ and $200M_\odot$ and dimensionless spin magnitudes of 0.9 and 0.8, respectively. The binary is placed at a redshift of 2, near the horizon of A+ detector with the developed technologies.

rate [71], normalized to a local merger rate density of 1 $\mathrm{Gpc}^{-3}\,\mathrm{yr}^{-1}$. We impose a detection threshold on the network SNR of $\rho_N \geq 12$. In Fig. 5(a), we show the fractional error on the detector frame masses as a function of redshift. The left panel shows the current A+ design with the present controls noise and the right panel the improvement that can be obtained when using the proposed upgraded configuration. For our assumed population, the upgraded configuration reduces the median Fisher uncertainty in the detector frame component masses by ≈50% relative to the current controls scheme, and by around ≈64% in the luminosity distance. We observe a relative increase of ≈86% in the fraction of detected binaries in our population. In addition, the 90th percentile of the detected redshift distribution increases from $z_{90} \simeq 1.49$ to $z_{90} \simeq 1.84$, corresponding to an increase of ≈1.47 in the enclosed comoving volume out to z_{90}. The low-frequency improvements provided by the developed technologies offer a significant increase in the cosmological reach of the detectors for low-mass IMBHs and opens up a new discovery space for high-mass IMBH sources.

To demonstrate the gain from the low-frequency improvements, we simulate an IMBH merger with component masses of $m_1 = 300M_\odot$ and $m_2 = 200M_\odot$, dimensionless spins of $\chi_1 = 0.9$ and $\chi_2 = 0.8$, and moderate spin-precession, $\chi_p = 0.5$ [72]. The binary is placed at a redshift of $z = 2$, sitting close to the horizon of the proposed detector as shown in Fig. 1. Assuming zero noise, the SNR is ≈9.2 compared to ≈3.9 in the presence of the current controls noise, where it falls below the detection threshold. To capture the full complexity of the signal near the merger regime, we use the NR surrogate model NRSur7dq4 [73] for both injection and recovery. We performed Bayesian inference using Bilby [74] and the nested sampling package DYNESTY [75]. The joint posterior probability distributions for a subset of parameters is shown in Fig. 5(b). Despite the challenging source being near the detection threshold, the proposed upgrade configuration resolves the total source frame mass to $M = 479^{+167}_{-112}$ and the redshift to $z = 1.7^{+0.9}_{-0.7}$. In contrast, the current controls noise provides no meaningful constraints, with the redshift being prior dominated. Such a clear observation of an IMBH would have profound implications for our understanding of black-hole formation channels, stellar evolution, and the growth of heavy black holes across cosmic time [1]. This discovery potential is driven by the improvements in low-frequency detector sensitivity outlined here.

Although we emphasize IMBHs as a compelling example, the low-frequency sensitivity improvements benefit compact-binary systems across the mass spectrum. Access to lower gravitational-wave frequencies extends the observable inspiral phase, since the time to merger scales as $t_{\rm merge} \propto f_{\rm GW}^{-8/3}$ [76]. Improved sensitivity below 30 Hz therefore increases the accumulated SNR, enhances parameter estimation, and enables earlier pre-merger localization for loud and nearby events. These gains strengthen multi-messenger opportunities and improve cosmological and population studies more broadly. A comprehensive discussion of the scientific impact of low-frequency sensitivity is given in Refs. [17,19].

Conclusions—In this Letter, we present three complementary technologies enabling substantial improvements in LIGO's low-frequency sensitivity to IMBHs. These technologies are required to approach the fundamental noise limits of current detectors and are critical for future upgrades and third-generation observatories. We characterize their noise performance and demonstrate their integration within the LIGO infrastructure, including active platform suppression tests at LIGO's MIT facility. We also achieve longitudinal platform suppression down to 10 mHz for the first time using C-6D. Propagating the impact of these technologies to detector strain sensitivity, we predict a

≈86% increase in detectable IMBH binaries. Additionally, we simulate an IMBH merger at redshift 2, demonstrating parameter constraints not achievable with LIGO's current isolation schemes.

Extending inertial isolation down to 10 mHz fundamentally shifts stabilization from suppressing vibrations to actively controlling slow drift. This has the potential to further advance the LIGO sensitivity [17], for example by increasing the inertia of the test masses and upgrading the suspension fibers [77], and reach the low-frequency facility limit determined by the gravity-gradient noise [78].

Apart from the gravitational-wave detectors, the developed technologies have the potential to unlock major gains across multiple precision fields [79]: in semiconductor lithography it can reduce low-frequency stage motion by one to two orders of magnitude, and along with more sensitive displacement sensing [80], improve overlay accuracy and enable smaller feature sizes [81]; in optical telescopes it can suppress slow structural and thermal distortions, improving pointing and wavefront stability and enhancing high-contrast imaging [82]; in quantum sensors and atomic interferometers it can reduce low-frequency acceleration noise, extending coherence times and enabling orders-of-magnitude sensitivity improvements [83,84]; and in electron microscopy and precision metrology it suppresses drift that currently limits resolution and long-duration measurements [85].

Acknowledgments—We acknowledge members of the LIGO Suspension Working Group for useful discussions, the support of the Institute for Gravitational Wave Astronomy at the University of Birmingham, STFC Consolidated Grant "Astrophysics at the University of Birmingham" (No. ST/S000305/1), UKRI Quantum Technology for Fundamental Physics scheme (Grants No. ST/T006609/1 and No. ST/W006375/1), and UKRI "The next-generation gravitational-wave observatory network" project (Grant No. ST/Y00423X/1). H. M. would like to acknowledge the support from the National Key R&D Program of China "Gravitational Wave Detection" (Grant No. 2023YFC2205800), and support from Quantum Information Frontier Science Center. A. S. U. thanks S. K. U. and A. K. U. for their encouragement and support.

Data availability—The data that support the findings of this article are not publicly available. The data are available from the authors upon reasonable request.

[1] J. E. Greene, J. Strader, and L. C. Ho, Annu. Rev. Astron. Astrophys. **58**, 257 (2020).
[2] R. Abbott, T. Abbott, S. Abraham, F. Acernese, K. Ackley, C. Adams, R. Adhikari, V. Adya, C. Affeldt, M. Agathos, K. Agatsuma, N. Aggarwal *et al.*, Phys. Rev. Lett. **125**, 101102 (2020).
[3] A. G. Abac, I. Abouelfettouh, F. Acernese, K. Ackley, C. Adamcewicz, S. Adhicary, D. Adhikari, N. Adhikari, R. X. Adhikari, V. K. Adkins, S. Afroz, A. Agapito, D. Agarwal *et al.*, Astrophys. J. Lett. **993**, L25 (2025).
[4] D. Gerosa and E. Berti, Phys. Rev. D **95**, 124046 (2017).
[5] P. Mahapatra, D. Chattopadhyay, A. Gupta, M. Favata, B. Sathyaprakash, and K. Arun, Phys. Rev. D **111**, 023013 (2025).
[6] D. Croon, J. Sakstein, and D. Gerosa, Mon. Not. R. Astron. Soc. **546**, stag073 (2026).
[7] K. Kremer, M. Spera, D. Becker, S. Chatterjee, U. N. Di Carlo, G. Fragione, C. L. Rodriguez, C. S. Ye, and F. A. Rasio, Astrophys. J. **903**, 45 (2020).
[8] G. Franciolini, K. Kritos, L. Reali, F. Broekgaarden, and E. Berti, Phys. Rev. D **110**, 023036 (2024).
[9] F. Antonini, I. Romero-Shaw, T. Callister, F. Dosopoulou, D. Chattopadhyay, M. Gieles, and M. Mapelli, Nat. Astron. (2026)..
[10] B. Abbott, R. Abbott, T. Abbott, M. Abernathy, F. Acernese, K. Ackley, C. Adams, T. Adams, P. Addesso, R. Adhikari, V. Adya, C. Affeldt, M. Agathos *et al.*, Phys. Rev. Lett. **116**, 061102 (2016).
[11] LIGO Scientific and Virgo Collaborations, Phys. Rev. X **9**, 031040 (2019).
[12] LIGO Scientific and Virgo Collaborations, Phys. Rev. X **11**, 021053 (2021).
[13] LIGO Scientific, Virgo, and KAGRA Collaborations, Phys. Rev. X **13**, 041039 (2023).
[14] LIGO Scientific, Virgo, and KAGRA Collaborations, ApJL **1004**, L22 (2026).
[15] B. Abbott, R. Abbott, T. Abbott, F. Acernese, K. Ackley, C. Adams, T. Adams, P. Addesso, R. Adhikari, V. Adya *et al.*, Phys. Rev. Lett. **119**, 161101 (2017).
[16] B. P. Abbott, R. Abbott, T. D. Abbott, F. Acernese, K. Ackley, C. Adams, T. Adams, P. Addesso, R. X. Adhikari, V. B. Adya *et al.*, Astrophys. J. Lett. **848**, L12 (2017).
[17] H. Yu, D. Martynov, S. Vitale, M. Evans, D. Shoemaker, B. Barr, G. Hammond, S. Hild, J. Hough, S. Huttner, S. Rowan, B. Sorazu, L. Carbone, A. Freise, C. Mow-Lowry, K. L. Dooley, P. Fulda, H. Grote, and D. Sigg, Phys. Rev. Lett. **120**, 141102 (2018).
[18] I. Gupta *et al.*, Classical Quantum Gravity **41**, 245001 (2024).
[19] E. D. Hall *et al.*, Phys. Rev. D **103**, 122004 (2021).
[20] B. P. Abbott, R. Abbott, T. D. Abbott, M. R. Abernathy, K. Ackley, C. Adams, P. Addesso, R. X. Adhikari, V. B. Adya, C. Affeldt *et al.*, Classical Quantum Gravity **34**, 044001 (2017).
[21] B. Sathyaprakash, M. Abernathy, F. Acernese, P. Ajith, B. Allen, P. Amaro-Seoane, N. Andersson, S. Aoudia, K. Arun, P. Astone *et al.*, Classical Quantum Gravity **29**, 124013 (2012).
[22] S. Hild, S. Chelkowski, A. Freise, J. Franc, N. Morgado, R. Flaminio, and R. DeSalvo, Classical Quantum Gravity **27**, 015003 (2009).
[23] F. Matichard *et al.*, Classical Quantum Gravity **32**, 185003 (2015).
[24] F. Matichard *et al.*, Precis. Eng. **40**, 273 (2015).
[25] F. Matichard *et al.*, Precis. Eng. **40**, 287 (2015).

[26] L. Carbone, S. M. Aston, R. M. Cutler, A. Freise, J. Greenhalgh, J. Heefner, D. Hoyland, N. A. Lockerbie, D. Lodhia, N. A. Robertson, C. C. Speake, K. A. Strain, and A. Vecchio, Classical Quantum Gravity **29**, 115005 (2012).
[27] S. J. Cooper, C. M. Mow-Lowry, D. Hoyland, J. Bryant, A. Ubhi, J. O'Dell, A. Huddart, S. Aston, and A. Vecchio, Rev. Sci. Instrum. **94**, 014502 (2023).
[28] D. Martynov *et al.*, Phys. Rev. D **93**, 112004 (2016).
[29] A. Buikema *et al.*, Phys. Rev. D **102**, 062003 (2020).
[30] E. Capote *et al.*, Phys. Rev. D **111**, 062002 (2025).
[31] D. Davis, T. Massinger, A. Lundgren, J. C. Driggers, A. L. Urban, and L. Nuttall, Classical Quantum Gravity **36**, 055011 (2019).
[32] See Supplemental Material at http://link.aps.org/supplemental/10.1103/65gz-dcjz for a breakdown of the BIS noise measurement, technical details of the active platform control, detector simulations, and astrophysical simulations.
[33] LIGO Scientific Collaboration, pyGWINC: Gravitational wave interferometer noise calculator, https://git.ligo.org/gwinc/pygwinc, accessed 2026.
[34] S. M. Aston *et al.*, Classical Quantum Gravity **29**, 235004 (2012).
[35] J. Buchli *et al.*, Science **389**, 1012 (2025).
[36] J. Smetana, R. Walters, S. Bauchinger, A. S. Ubhi, S. Cooper, D. Hoyland, R. Abbott, C. Baune, P. Fritchel, O. Gerberding, S. Köhnke, H. Miao, S. Rode, and D. Martynov, Phys. Rev. Appl. **18**, 034040 (2022).
[37] J. Smetana, C. Di Fronzo, A. Amorosi, and D. Martynov, Sensors **23**, 7526 (2023).
[38] O. Gerberding, Opt. Express **23**, 14753 (2015).
[39] G. Heinzel, F. Guzmán Cervantes, A. F. García Marin, J. Kullmann, W. Feng, and K. Danzmann, Opt. Express **18**, 19076 (2010).
[40] E. Wielandt and G. Streckeisen, Bull. Seismol. Soc. Am. **72**, 2349 (1982), https://pubs.geoscienceworld.org/ssa/bssa/article-abstract/72/6A/2349/118472/The-leaf-spring-seismometer-Design-and-performance.
[41] C. M. Mow-Lowry and D. Martynov, Classical Quantum Gravity **36**, 245006 (2019).
[42] A. S. Ubhi, J. Smetana, T. Zhang, S. Cooper, L. Prokhorov, J. Bryant, D. Hoyland, H. Miao, and D. Martynov, Classical Quantum Gravity **39**, 015006 (2021).
[43] A. S. Ubhi, L. Prokhorov, S. Cooper, C. D. Fronzo, J. Bryant, D. Hoyland, A. Mitchell, J. van Dongen, C. Mow-Lowry, A. Cumming, G. Hammond, and D. Martynov, Appl. Phys. Lett. **121**, 174101 (2022).
[44] L. Prokhorov, S. Cooper, A. S. Ubhi, C. Mow-Lowry, J. Bryant, A. Dmitriev, C. Di Fronzo, C. J. Collins, A. Gill, A. Mitchell, J. Heinze, J. Smetana, T. Yan, A. V. Cumming, G. Hammond, and D. Martynov, Phys. Rev. D **109**, 042007 (2024).
[45] J. Smetana, A. S. Ubhi, E. Chick, L. Prokhorov, J. Bryant, A. Dmitriev, A. Gill, L. Koponen, D. Martynov, H. Miao, A. V. Cumming, G. Hammond, V. Frolov, R. Mittleman, and P. Fritchel, Phys. Rev. Appl. **23**, 024013 (2025).
[46] A. V. Cumming, A. S. Bell, L. Barsotti, M. A. Barton, G. Cagnoli, D. Cook, L. Cunningham, M. Evans, G. D. Hammond, G. M. Harry, A. Heptonstall, J. Hough, R. Jones, R. Kumar, R. Mittleman, N. A. Robertson, S. Rowan, B. Shapiro, K. A. Strain, K. Tokmakov, C. Torrie, and A. A. van Veggel, Classical Quantum Gravity **29**, 035003 (2012).
[47] P. G. Nelson, Rev. Sci. Instrum. **62**, 2069 (1991).
[48] S. J. Richman, J. A. Giaime, D. B. Newell, R. T. Stebbins, P. L. Bender, and J. E. Faller, Rev. Sci. Instrum. **69**, 2531 (1998).
[49] J. M. Hensley, A. Peters, and S. Chu, Rev. Sci. Instrum. **70**, 2735 (1999).
[50] W. Hakvoort, G. Boerrigter, and M. Beijen, IFAC-PapersOnLine **53**, 9144 (2020).
[51] T. Wang, C. Blair, A. Al-Jodah, J. Winterflood, J. Liu, A. Adams, A. Goodwin-Jones, C. Zhao, and L. Ju, Rev. Sci. Instrum. **96**, 064504 (2025).
[52] F. Matichard and M. Evans, Bull. Seismol. Soc. Am. **105**, 497 (2015).
[53] F. Matichard, M. Evans, R. Mittleman, M. MacInnis, S. Biscans, K. L. Dooley, H. Sohier, A. Lauriero, H. Paris, J. Koch, P. Knothe, A. Carbajo, and C. Dufort, Rev. Sci. Instrum. **87**, 065002 (2016).
[54] M. P. Ross, K. Venkateswara, C. Mow-Lowry, S. Cooper, J. Warner, B. Lantz, J. Kissel, H. Radkins, T. Shaffer, R. Mittleman, A. Pele, and J. Gundlach, Classical Quantum Gravity **37**, 185018 (2020).
[55] S. Soni *et al.*, Classical Quantum Gravity **42**, 085016 (2025).
[56] J. A. Sidles and D. Sigg, Phys. Lett. A **354**, 167 (2006).
[57] J. Liu, V. Bossilkov, C. Blair, C. Zhao, L. Ju, and D. G. Blair, Rev. Sci. Instrum. **89**, 124503 (2018).
[58] G. D. Meadors, K. Kawabe, and K. Riles, Classical Quantum Gravity **31**, 105014 (2014).
[59] E. Capote and J. Driggers (LIGO Scientific Collaboration), Overview of interferometer sensing and control, Technical Report No. LIGO-G2300437-v1, LIGO Laboratory, 2023 (created: 03 March 2023; Metadata Revised: 02 May 2024; Accessed: 12 February 2026).
[60] A. Buonanno and Y. Chen, Phys. Rev. D **65**, 042001 (2002).
[61] A. C. Green, D. D. Brown, M. Dovale-Álvarez, C. Collins, H. Miao, C. M. Mow-Lowry, and A. Freise, Classical Quantum Gravity **34**, 205004 (2017).
[62] C. Reissel, D. Lai, S. Dwivedi, E. Bonilla, C. Geer, C. Wipf, R. Mittleman, P. Harris, E. Schwartz, D. Poznanski, B. Lantz, and E. Katsavounidis, Microseismic noise mitigation with machine learning for Advanced LIGO, arXiv:2511.19682.
[63] G. Heinzel, K. A. Strain, J. Mizuno, K. D. Skeldon, B. Willke, W. Winkler, R. Schilling, A. Rüdiger, and K. Danzmann, Phys. Rev. Lett. **81**, 5493 (1998).
[64] A. Longo, S. Bianchi, G. Valdes, N. Arnaud, and W. Plastino, Classical Quantum Gravity **39**, 035001 (2021).
[65] S. Soni *et al.* (LIGO Scientific Collaboration), Classical Quantum Gravity **38**, 025016 (2021).
[66] A. Staley *et al.*, Classical Quantum Gravity **31**, 245010 (2014).
[67] LIGO Scientific Collaboration, Inspiral range calculator, https://git.ligo.org/gwinc/inspiral-range (accessed 2026).
[68] U. Dupletsa, J. Harms, B. Banerjee, M. Branchesi, B. Goncharov, A. Maselli, A. C. S. Oliveira, S. Ronchini, and J. Tissino, Astron. Comput. **42**, 100671 (2023).

[69] G. Pratten, S. Husa, C. Garcia-Quiros, M. Colleoni, A. Ramos-Buades, H. Estelles, and R. Jaume, Phys. Rev. D **102**, 064001 (2020).
[70] C. García-Quirós, M. Colleoni, S. Husa, H. Estellés, G. Pratten, A. Ramos-Buades, M. Mateu-Lucena, and R. Jaume, Phys. Rev. D **102**, 064002 (2020).
[71] P. Madau and M. Dickinson, Annu. Rev. Astron. Astrophys. **52**, 415 (2014).
[72] P. Schmidt, F. Ohme, and M. Hannam, Phys. Rev. D **91**, 024043 (2015).
[73] V. Varma, S. E. Field, M. A. Scheel, J. Blackman, L. E. Kidder, and H. P. Pfeiffer, Phys. Rev. D **99**, 064045 (2019).
[74] G. Ashton *et al.*, Astrophys. J. Suppl. Ser. **241**, 27 (2019).
[75] J. S. Speagle, Mon. Not. R. Astron. Soc. **493**, 3132 (2020).
[76] J. D. E. Creighton and W. G. Anderson, *Gravitational-Wave Physics and Astronomy: An Introduction to Theory, Experiment and Data Analysis* (Wiley, New York, 2011), 10.1002/9783527636037.
[77] B. Lantz *et al.*, LIGO A#—Post O5 upgrade and step toward Cosmic Explorer, Technical document, LIGO Document Control Center, 2024 (accessed: 2026-02-13), https://dcc.ligo.org/LIGO-G2301738/public.
[78] S. A. Hughes and K. S. Thorne, Phys. Rev. D **58**, 122002 (1998).
[79] C. Collette, S. Janssens, K. Artoos, and C. Hauviller, Diamond Light Source Proc. **1**, e1 (2010).
[80] S. Scott and K. Stephen, *Handbook of Optical Dimensional Metrology* (CRC Press, Boca Raton, 2016), pp. 108–171.
[81] Y. Song, C. Gui, Z. Huo, S. W. R. Lee, and S. Liu, Int. J. Mech. Syst. Dyn. **1**, 35 (2021).
[82] J. Leon-Gil, J. Gonzalez-Cava, A. Zamora-Jimenez, M. Nuñez-Cagigal, and J. Mendez-Perez, IFAC-PapersOnLine **59**, 184 (2025).
[83] D. Xie, S. Yan, L. Zhu, H. Zhang, and X. Zhang, J. Phys. Conf. Ser. **2125**, 012022 (2021).
[84] F. Oon and R. Dumke, Phys. Rev. Appl. **18**, 044037 (2022).
[85] Y.-H. Shin, S.-J. Moon, Y.-J. Kim, and K.-Y. Oh, Sensors **20**, 2277 (2020).